Surface & Coatings Technology 203 (2009) 1114–1120

Contents lists available at ScienceDirect

Surface & Coatings Technology

journal homepage: www.elsevier.com/locate/surfcoat

On the thermally induced cracking of a segmented coating deposited on the outer surface of a hollow cylinder

Xuejun Chen [a,b,*], Guangnan Chen [b]

[a] School of Applied Sciences, University of Science and Technology Beijing, No. 30 Xueyuan Road, Beijing 100083, PR China
[b] Institute of Mechanics, Chinese Academy of Sciences, Beijing 100080, PR China

ARTICLE INFO

Article history:
Received 23 August 2008
Accepted in revised form 1 October 2008
Available online 14 October 2008

Keywords:
Segmented coating
Cracking
Thermal Stress Intensity Factor (TSIF)
Finite element method

ABSTRACT

In this work, the thermally induced cracking behavior of a segmented coating has been investigated. The geometry under consideration is a hollow cylinder with a segmented coating deposited onto its outer surface. The segmentation cracks are modeled as a periodic array of axial edge cracks. The finite element method is utilized to obtain the solution of the multiple crack problem and the Thermal Stress Intensity Factors (TSIFs) are calculated. Based on dimensional analysis, the main parameters affecting TSIFs are identified. It has been found that the TSIF is a monotonically increasing function of segmentation crack spacing. This result confirms that a segmented coating exhibits much higher thermal shock resistance than an intact counterpart, if only the segmentation crack spacing is narrow enough. The dependence of TSIF on some other parameters, such as normalized time, segmentation crack depth, convection severity as well as material constants, has also been discussed.

1. Introduction

The thermally induced failure problem of a hollow cylinder is an important issue for designing and manufacturing of such structural components as pressure vessels and pipes. To enhance a certain surface properties (e.g., thermal, corrosion or wear resistance) of the wall materials, protective coatings are widely used in many modern applications. Unfortunately, disadvantageous problems have also been brought about, one of which is the surface cracking of coating [1]. In the absence of additional loads and because of self-equilibrating nature of the thermal stress state, the cracking may not always lead to a through-thickness fracture. However, once the surface crack penetrates the coating-substrate interface, interfacial debonding may occur subsequently [2]. On the other hand, surface cracks touching on interface will act as convenient tunnels for corrosive gases, by which the substrate and the interface are attacked [3]. This situation poses a major threat to the integrity of the entire coating-substrate system since it will result in final removal of coating.

Therefore, it is of great importance to delay the surface crack growth in an effort to prolong the total fatigue life of the coated components. This requires the calculation of the crack driving force for the given thermal loads as a function of the crack depths and material constants. Although thermally induced cracking analysis has been widely performed for homogeneous cylinders [4–10], the similar study concerning coated cylinders seems relatively limited. In the early 1980s, an analysis for nuclear pressure vessel application was presented in Ref. [11], which demonstrated the important role that a cladding layer played in the thermal shock resistance of a circumferentially cracked hollow cylinder. Based on the solution of singular integral equations, the transient thermal stress problem in a coated hollow cylinder containing a single radial crack was considered by Tang and Erdogan [12]. A modified elimination finite element scheme was developed by Chen and Kuo [13] to investigate the transient thermo-elastic behavior of a two-layer annular cylinder with an internal edge crack subjected to a sudden heating. Recently, the transient thermal stress intensity problem of an inner-coated hollow cylinder with multiple pre-existing surface cracks contained in the coating has been studied [14].

In parallel efforts, various coating designs were proposed to accommodate the misfit strain between the coating and substrate, such as functionally gradient coating, duplex coating as well as multilayer coating [15–17]. In contrast to the aforementioned ideas of an intact coating, a new concept of coating design, i.e. the segmented coating, has been recently developed to enhance the durability of coating in a fluctuating thermal environment [18–20]. Herein, the segmented coating refers to a coating with periodic segmentation cracks running from the surface of coating toward the interface of coating/substrate. One of such segmented coating (after a few thermal cycles) is shown in Fig. 1, which was prepared by the hybrid technique of laser discrete pre-quenching substrate plus post-deposition [21].

It should be noted that the spacing of the formed segmentation cracks can be controlled by adjusting the hybrid processing parameters, the details of which can be found elsewhere [20]. Experimental observations [20] demonstrated that the segmented coating exhibited

* Corresponding author. School of Applied Sciences, University of Science and Technology Beijing, No. 30 Xueyuan Road, Beijing 100083, PR China. Tel.: +86 10 62332985; fax: +86 10 62327283.
E-mail address: chenxuejuncas@sohu.com (X. Chen).

0257-8972/$ – see front matter © 2008 Elsevier B.V. All rights reserved.
doi:10.1016/j.surfcoat.2008.10.002

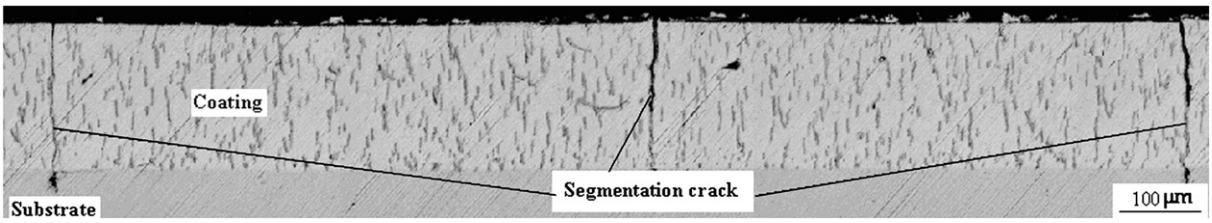

Fig. 1. The profile of a typical segmented coating [21]. (The periodic segmentation cracks were formed by the hybrid technique of laser discrete pre-quenching substrate plus post-deposition.)

more thermal-shock-bearing capacity than the intact coating. In fact, such a beneficial effect has also been reported in previous literature [22,23], in which the benefit was attributed to misfit strain level alleviation resulted from in-plane compliance increase of a pre-cracked coating. The main purpose of this paper is to apply such a segmented coating to an outer-surface-coated hollow cylinder and to reveal the underlying mechanism from the standpoint of fracture mechanics.

In this paper, the thermally induced cracking behavior of a segmented coating on the outer surface of a hollow cylinder has been reported. The cylinder is assumed to be exposed to convective heating from the inner surface while the outer surface is perfectly insulated. It should be noted that, for a finitely long cylinder the thermal stress analyses are usually complicated 3-D problems and a crack may propagate in axial or circumferential as well as in the thickness direction. For simplicity, the cylinder in question is modeled as a plane strain problem and the segmentation cracks are modeled as a periodic array of axial edge cracks. This simplification is considered to represent a reasonable idealization for the stresses and displacements in the central portion of a long cylinder to provide an upper bound solution [12]. In this analysis, both coating and substrate materials are taken to be homogeneous, isotropic and linear-elastic, the thermo-mechanical constants are independent of temperature, and the thermo-elastic coupling effects and inertia effects are negligible. Previous investigations on dynamic thermo-elasticity seemed to support the validity of the last assumption [24,25].

The paper is organized as follows. The transient thermal stress field for the un-cracked hollow cylinder is established in Section 2. In Section 3, taking advantage of the assumed linearity of the materials, the principle of superposition is adopted. The solution of the multiple crack problem is obtained by utilizing the calculated transient thermal stresses in Section 2 with opposite sign on the crack surfaces as the only crack surface tractions. In Section 3, the transient thermal stress intensity factors (TSIFs) are also evaluated using finite element (FE) method. In Section 4, the main parameters affecting TSIFs are identified based on dimensional analysis. The numerical results for the TSIFs are obtained in Section 5 as a function of normalized quantities such as time, convection severity, segmentation crack spacing, segmentation crack length as well as material constants. Finally, main conclusions of the present investigation are drawn in Section 6.

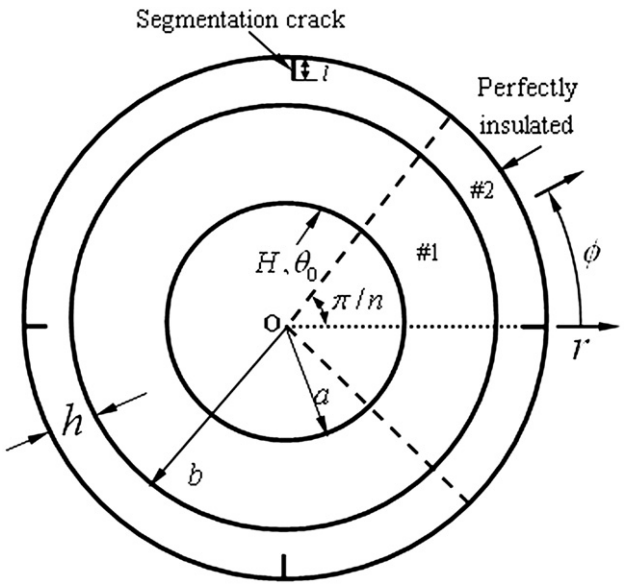

Fig. 2. The segmented coating-substrate system subjected to convective heating from inner surface.

2. Thermal stresses in the un-cracked cylinder

The problem of an outer-surface-coated hollow cylinder under consideration is depicted in Fig. 2, with the origin of cylindrical coordinates (r, ϕ, z) at its center. The substrate cylinder (material #1) has an inner radius a and an outer radius b. The segmented coating (material #2) of thickness h contains n uniformly spaced, radially oriented segmentation cracks of depth l (Only four segmentation cracks are plotted in Fig. 2.).

Let the temperature in the substrate and coating be T_1 and T_2, respectively. As the un-cracked medium is axisymmetric, there is no variation of temperature in the circumferential direction. Therefore, T_1 and T_2 would be functions of radial coordinate r and the time t only. The temperature deviations $\theta_i(r,t)$ are defined by

$$\theta_i(r,t) = T_i(r,t) - T_0 \quad (i = 1,2) \tag{1}$$

The subscripts 1 and 2 refer to substrate and coating, respectively. T_0 is the initial homogeneous temperature of the coated cylinder.

Since the segmentation cracks are assumed in the radial direction, the hoop stresses of un-cracked cylinders are of primary interest because they determine the propagation of the crack in mode I fracture [12]. The hoop stress for the problem, under the assumption of plane strain conditions, can be expressed as [12]:

$$\sigma_{\phi\phi i}(r,t) = \frac{\alpha_i E_i}{1-\nu_i}\frac{1}{r^2}\int_{a_i}^{r}\theta_i(\rho,t)\rho d\rho - \frac{\alpha_i E_i}{1-\nu_i}\theta_i(r,t) + \frac{E_i}{1+\nu_i}\left(\frac{C_{1i}}{1-2\nu_i} + \frac{C_{2i}}{r^2}\right) \tag{2}$$

where $i=1,2$, $a_i=a$ for $i=1$; $a_i=b$ for $i=2$. The symbols α, E and ν denote coefficient of thermal expansion (CTE), Young's modulus, and Poisson's ratio respectively. The unknown constants C_{1i}, C_{2i} are determined from the following boundary and continuity conditions.

$$\sigma_{rr1}(a,t) = 0; \quad \sigma_{rr2}(b+h,t) = 0 \quad (t > 0) \tag{3a}$$

$$u_{r1}(b,t) = u_{r2}(b,t); \quad \sigma_{rr1}(b,t) = \sigma_{rr2}(b,t) \quad (t > 0) \tag{3b}$$

To obtain the temperature distributions θ_1 and θ_2, the following heat diffusion equations should be solved for given initial and boundary conditions.

$$\nabla^2\theta_i(r,t) = \frac{1}{D_i}\frac{\partial\theta_i(r,t)}{\partial t} \quad (i = 1,2) \tag{4}$$

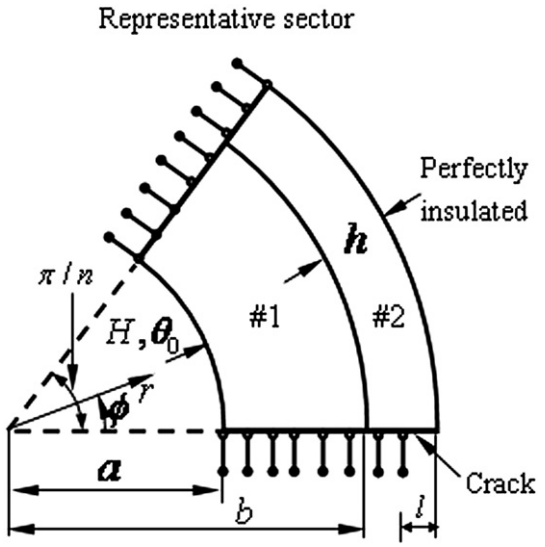

Fig. 3. A representative section of segmented coating-substrate with central angle of π/n.

The thermal diffusivity D is given by $D=k/\rho c$, where k is the material thermal conductivity, ρ the density, c the specific heat and $\nabla^2=\partial^2/\partial r^2+r^{-1}\partial/\partial r$.

At time $t=0$, the inner surface is subjected to convective heating with the heat transfer coefficient H and the ambient temperature maintained at T_a while the outer surface is kept perfectly insulated. Thus the initial conditions are given by

$$\theta_1(r,0)=0 \quad (a\le r\le b); \quad \theta_2(r,0)=0 \quad (b\le r\le b+h) \tag{5a}$$

The continuity and boundary conditions are written as

$$\theta_1(b,t)=\theta_2(b,t), \quad k_1\frac{\partial}{\partial r}\theta_1(b,t)=k_2\frac{\partial}{\partial r}\theta_2(b,t) \quad (t>0) \tag{5b}$$

$$\frac{\partial}{\partial t}\theta_1(a,t)=\frac{H}{k_1}\left[\theta_1(a,t)-\theta_0\right] \quad \frac{\partial}{\partial r}\theta_2(b+h,t)=0 \quad (t>0) \tag{5c}$$

where $\theta_0=T_a-T_0$, in the case of convective heating, $\theta_0>0$. Eq. (3b) indicates that the temperature and heat flux are assumed to be continuous at the bonded interface, neglecting contact thermal resistance. The diffusion equation is solved by using the standard Laplace transform technique [26].

3. The stress intensity factors

As the result of thermal stresses, at any time instant the stress intensity builds up around the segmentation crack tip. Based on the principle of superposition, the thermal stress problem for a coated hollow cylinder containing multiple radial cracks may now be solved by using the equal and opposite of the hoop stress given by Eq. (2) as the crack surface traction. In the case of n segmentation cracks evenly spaced and of equal depth l, only a representative sector with a central angle of π/n, has to be considered, as shown in Fig. 3. The surfaces $r=a$, $r=b+h$ and $\phi=\pi/n$ of the representative sector are subjected to the following homogeneous boundary conditions

$$\sigma_{rr1}(a,\phi,t)=\sigma_{r\phi1}(a,\phi,t)=0 \quad (0<\phi<\pi/n, t>0) \tag{6a}$$

$$\sigma_{rr2}(b+h,\phi,t)=\sigma_{r\phi2}(b+h,\phi,t)=0 \quad (0<\phi<\pi/n, t>0) \tag{6b}$$

$$u_{\phi1}(r,\pi/n,t)=u_{\phi2}(r,\pi/n,t)=0 \quad (a<r<b+h, t>0) \tag{6c}$$

The continuity conditions on the interface of coating and substrate read

$$u_{r1}(b,\phi,t)=u_{r2}(b,\phi,t); u_{\phi1}(b,\phi,t)=u_{\phi2}(b,\phi,t) \quad (0<\phi<\pi/n, t>0) \tag{6d}$$

$$\sigma_{rr1}(b,\phi,t)=\sigma_{rr2}(b,\phi,t); \sigma_{r\phi1}(b,\phi,t)=\sigma_{r\phi2}(b,\phi,t) \quad (0<\phi<\pi/n, t>0) \tag{6e}$$

There are following additional mixed boundary conditions on the plane of $\phi=0$:

$$u_{\phi1}(r,0,t)=u_{\phi2}(r,0,t)=0 \quad \sigma_{r\phi}(a,\phi,t)=0 \quad (a<r<b+h-l, t>0) \tag{6f}$$

$$\sigma_{\phi\phi}(r,+0,t)=\sigma_0(r,t) \quad \sigma_{r\phi}(r,+0,t)=0 \quad (b+h-l<r<b+h, t>0) \tag{6g}$$

where σ_{jk} ($j, k=r, \phi$) and u_j are the stresses and the displacement, respectively. $\sigma_0(r,t)$ is the pseudo-traction, which has the equal value of thermal stress from the un-cracked problem, given by Eq. (2) but with an opposite sign.

Since the transient mixed boundary problem is analytically intractable, it has been solved via FE method by using the commercial finite element package ANSYS [27]. Eight-node isoparametric quadrilateral elements have been used for displacement calculations. Each of the sectors has been divided into 1150–8676 elements in terms of different crack numbers. In order to obtain accurate results, careful element meshing has been considered to assure a reasonable aspect

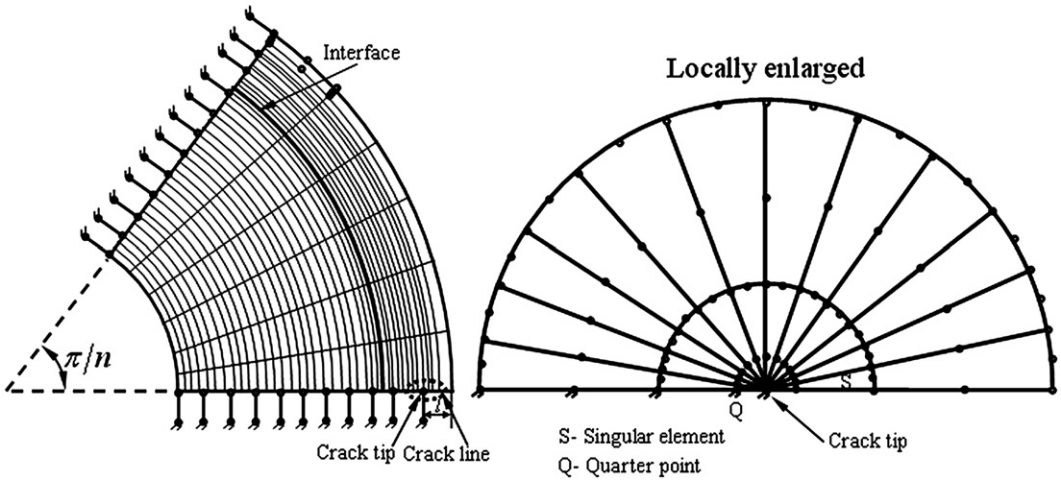

Fig. 4. Finite element meshes in the analysis (dimensions are not in proportion).

Table 1
The dimensionless quantities used in this analysis [30]

D_2/D_1	k_2/k_1	E_2/E_1	υ_2/υ_1	α_2/α_1	a/h	b/h
0.730	0.632	0.317	1.064	0.608	80	100

ratio of the elements, and particularly element refinements have been carried out in the vicinity of the crack tip and the interface of coating and substrate. The detailed mesh configuration is schematically illustrated in Fig. 4.

In linear elastic problems, it has been shown that the displacements near the crack tip vary as $\sqrt{r}$, where r is the distance from the crack tip. The stresses and strains are singular at the crack tip, varying as $1/\sqrt{r}$. To pick up the singularity in the strain, the crack faces should be coincident, and the elements around the crack tip should be quadratic, with mid-side nodes placed at the quarter points, known as singular elements. The quarter points and the singular elements surrounding the crack tip are labeled in Fig. 4 as Q and S respectively. The first row of elements around the crack tip should be singular, the radius of which is chosen to be one tenth of quadrilateral element length, and the number of elements in the local circumferential direction is twelve. The stress intensity factor is extracted from the FE solution via the circumferential displacement $u\phi$ at the quarter point of the singular element on the free face of the crack. This relation can be expressed as [28]

$$K_I = \frac{E_i u_\phi}{(1+\nu_i)(1+\kappa_i)}\sqrt{\frac{2\pi}{r_q}} \tag{7}$$

where r_q is the distance from quarter point to the crack tip, $i=1$ when the crack tip is within the substrate while $i=2$ within the coating and $\kappa_i = 3-4\nu_i$ in the case of plane strain problem.

4. Dimensional analysis

To properly describe the coating-substrate responses, dimensional analysis can be utilized to derive the predominant dimensionless parameters from the parameters involved. The temperature deviations θ_i ($i=1,2$) must be functions of the following independent governing parameters: temporal and spatial coordinates t and r; characteristic geometrical parameters a, b and h; thermo-physical constants D_1, D_2, k_1, k_2; heat transfer coefficient H and ambient temperature deviations θ_0

$$\theta_i(r,t) = \theta_i(r,t;a,b,h;D_1,D_2,k_1,k_2;H,\theta_0) \tag{8}$$

Among the eleven governing parameters, four of them, namely h, D_1, k_1 and θ_0, have independent dimensions. The dimensions of θ_i, r, t, a, b, D_2 and k_2 are given by

$$\begin{aligned}&[\theta_i]=[\theta_0] \quad [r]=[h] \quad [t]=[D_1]^{-1}[h]^2\\ &[a]=[b]=[h] \quad [D_2]=[D_1] \quad [k_2]=[k_1] \quad H=[k_1][h]^{-1}\end{aligned} \tag{9}$$

On applying Π-theorem in dimensional analysis [29], a functional relationship can be established as

$$\frac{\theta_i}{\theta_0} = \Pi_\theta\left(\frac{r}{h},\frac{D_1 t}{h^2};\frac{a}{h},\frac{b}{h};\frac{D_2}{D_1},\frac{k_2}{k_1};\frac{Hh}{k_1}\right) \tag{10}$$

The following dimensionless quantities are then naturally defined as

$$\begin{aligned}&\bar{r}=\frac{r}{h} \quad \mathrm{Fo}=\frac{D_1 t}{h^2} \quad \bar{a}=\frac{a}{h} \quad \bar{b}=\frac{b}{h}\\ &\bar{D}=\frac{D_2}{D_1} \quad \bar{k}=\frac{k_2}{k_1} \quad \mathrm{Bi}=\frac{Hh}{k_1}\end{aligned} \tag{11}$$

Based on the above dimensional analysis, the dimensionless quantity θ_i/θ_0 on the left side of Eq. (10) is determined only by seven dimensionless quantities on the right side, in which Bi and Fo are similar to conventional Biot number and Fourier number, respectively.

In a similar manner, normalized thermal stress components depend on the following dimensionless quantities,

$$\frac{(1-\nu_1)\sigma}{E_1\alpha_1\theta_0} = \Pi_\sigma\left(\frac{r}{h},\frac{D_1 t}{h^2};\frac{a}{h},\frac{b}{h};\frac{D_2}{D_1},\frac{k_2}{k_1},\frac{Hh}{k_1};\frac{E_2}{E_1},\frac{\nu_2}{\nu_1},\frac{\alpha_2}{\alpha_1}\right) \tag{12}$$

It can be shown that, three additional dimensionless material quantities, $\bar{E}=E_2/E_1$, $\bar{\nu}=\nu_2/\nu_1$ and $\bar{\alpha}=\alpha_2/\alpha_1$ should appear in thermal stress analysis, which measure substrate and coating's relative value of Young's modulus, Poisson's ratio and coefficient of thermal expansion (CTE) respectively.

In terms of time-dependent thermal stress, the mode I stress intensity factor (TSIF) for multiple segmentation cracks is also time-dependent. Furthermore, crack depth l and crack spacing s, which characterize multiple segmentation crack configuration, should be added into corresponding function,

$$K(t) = g(t,\theta_0;a,b,h,;D_1,D_2,k_1,k_2,H;E_1,E_2,\nu_1,\nu_2,\alpha_1,\alpha_2;l,s) \tag{13}$$

On applying Π-theorem again, the TSIFs can be of the dimensionless form

$$\frac{(1-\nu_1)K}{E_1\alpha_1\theta_0\sqrt{h}} = \Pi_K\left(\frac{D_1 t}{h^2};\frac{a}{h},\frac{b}{h};\frac{D_2}{D_1},\frac{k_2}{k_1},\frac{Hh}{k_1};\frac{E_2}{E_1},\frac{\nu_2}{\nu_1},\frac{\alpha_2}{\alpha_1};\frac{l}{h},\frac{s}{h}\right) \tag{14}$$

where $s \equiv 2\pi(b+h)/n$ is the segmentation crack spacing and n the crack number. With the help of the above dimensional analysis, sensitivity analysis for temperature, thermal stress and TSIF can be conveniently performed, which will be detailed in Section 5.

5. Results and discussions

As an example for the thermally induced cracking problem of a segmented coating described in the previous sections, a material pair, which corresponds to an Al_2O_3 ceramic coating and a stainless steel substrate, has been considered. Since the problem is formulated in terms of dimensionless quantities, it is sufficient to consider only the ratios of material constants shown in Table 1. Unless otherwise stated, the data in our calculations are taken from Table 1. All the quantities of interest are normalized in the same forms as those in Section 4.

Selected results concerning transient temperature and thermal stresses for an un-cracked hollow cylinder are displayed in Figs. 5 and 6, respectively. The normalized temperature is plotted against

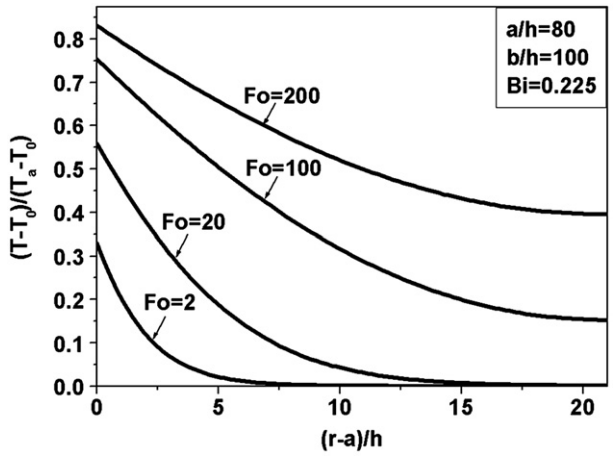

Fig. 5. The normalized temperature versus normalized radial coordinate, for various dimensionless time instants. Bi=0.225, $a/h=80$, $b/h=100$ and other inputs are listed in Table 1.

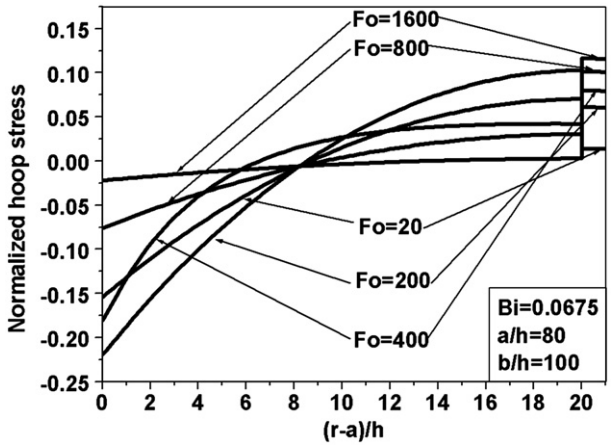

Fig. 6. The normalized hoop stress versus normalized radial coordinate for various time instants. Bi = 0.0675, $a/h = 80$, $b/h = 100$. Other inputs are listed in Table 1.

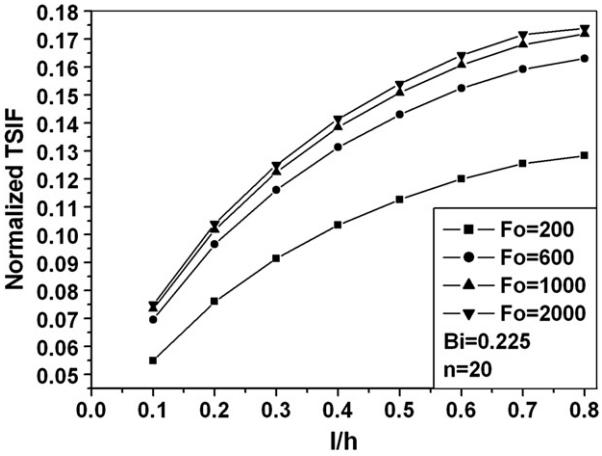

Fig. 8. The normalized TSIF versus normalized segmentation crack depth for various normalized time. Bi = 0.225, $n = 20$. Other inputs are listed in Table 1.

normalized radial coordinate in Fig. 5 for various dimensionless time, Fo = 2, 20, 100, 200. In this plot, the Biot number is taken as 0.225. It has been shown that at a certain time instant, the normalized temperature decreases as the distance from the inner surface increases; while at a fixed location, the normalized temperature increases with the elapse of time.

In Fig. 6, the variation of the normalized hoop stress in an uncracked cylinder versus normalized radial coordinate has been presented for different normalized time, Fo = 20, 200, 400, 800, 1600. It can be seen that the coating invariably experiences tensile hoop stress. In terms of the differences in thermo-physical properties of coating and substrate, hoop stress discontinues at the interface as expected. Due to the self-equilibrating nature of thermal stress, there exists a compressive stress region somewhere near the inner surface. This trend is in agreement with corresponding normalized temperature distribution in Fig. 5. It can also be seen that the normalized hoop stress distribution in the coating is almost uniform.

Selected results of crack driving force, represented by mode I thermal stress intensity factor (TSIF), are shown in Figs. 7–12. First, by considering same material constants (i.e. homogeneous hollow cylinder) for coating and substrate, a series of runs have been performed to duplicate various results of double external axial cracks by Oliveira and Wu [6], which was obtained by using a closed-form weight function. Most of the results were found to be in excellent agreement with those in the reference (see Table 2). Hence, the present FE model is reasonably validated.

In Fig. 7, the normalized TSIF versus normalized time for various normalized segmentation crack depth is plotted. In this graph, the segmentation crack number is taken to be ten and the Biot number is 0.225. It can be seen that, for a given crack depth, the normalized TSIF increases monotonically with time until the steady state is reached. Therefore the maximum TSIF is approached at steady state of thermal transients. In terms of the current input data in Table 1, the thermal steady state is reached at approximately Fo = 2000.

Fig. 8 shows the variation of the TSIF with the segmentation crack depth, at different time Fo = 200, 600, 1000, 2000. The crack number is fixed as $n = 20$. It can be seen that, as the normalized segmentation crack depth increases, the normalized TSIF also increases at any instant. This variation trend is the consequence of "uniform distribution" feature of corresponding hoop stress distribution within coating, as shown in Fig. 6. The above information enables one to conclude that, at any fixed instant, once the TSIF of the segmentation crack is high enough to exceed the fracture toughness of the coating, it will propagate unstably in the coating.

The influence of convection severity measured by Biot number on the TSIF can be induced from Fig. 9. As more severe thermal transient is applied (with the same ambient temperature), the maximum TSIF occurs earlier while the magnitude of maximum TSIF is kept unchanged.

The variation of normalized TSIF versus normalized segmentation crack spacing $\bar{s} = s/h$ for various segmentation crack depth is depicted in Fig. 10. Since the segmentation crack density is inversely related to

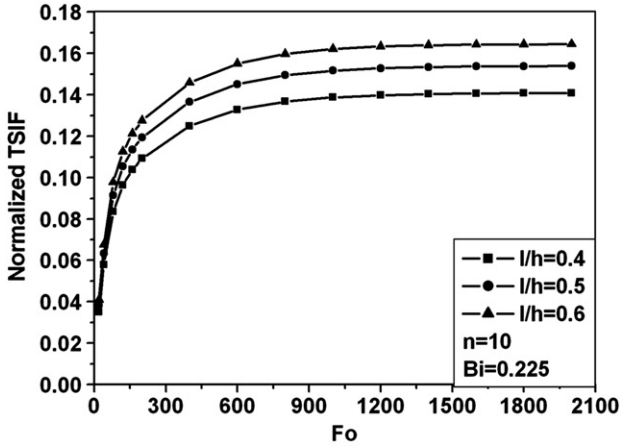

Fig. 7. The normalized TSIF versus normalized time for various normalized segmentation crack depth. Bi = 0.225, $n = 10$. Other inputs are listed in Table 1.

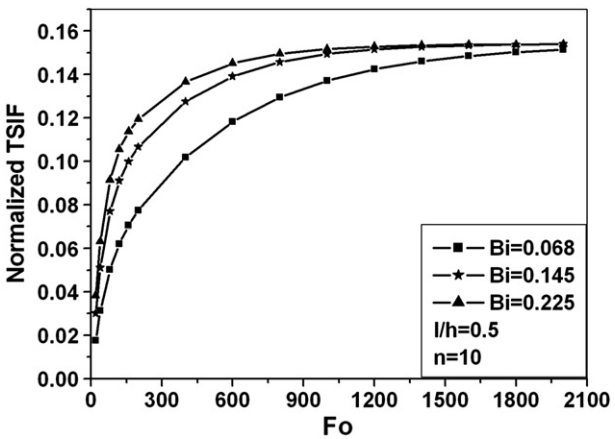

Fig. 9. The normalized TSIF versus normalized time for various convection severity. $l/h = 0.5$, $n = 10$. Other inputs are listed in Table 1.

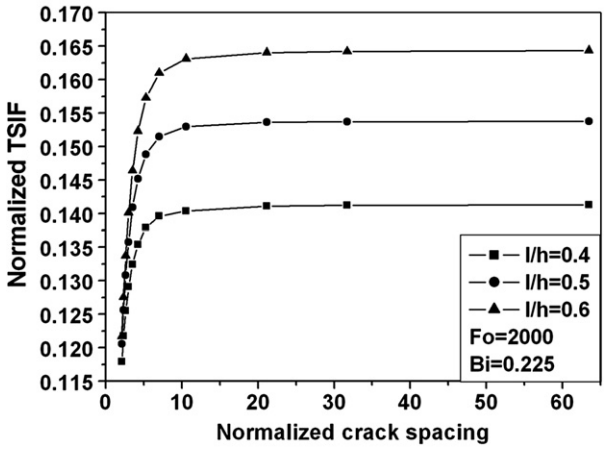

Fig. 10. The normalized TSIF versus normalized segmentation crack spacing for various normalized crack depth. Fo=2000, Bi=0.225. Other inputs are listed in Table 1.

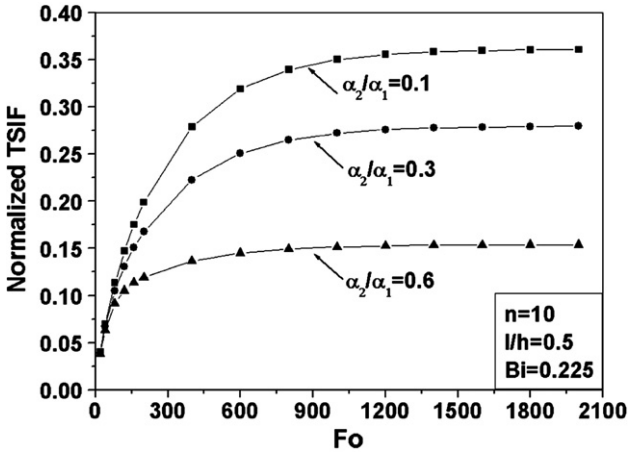

Fig. 12. The normalized TSIF versus normalized time for various CTE ratio. $l/h=0.5$, $n=10$, Bi=0.225. Other inputs are listed in Table 1.

the segmentation crack spacing, this graph actually represents the dependence of segmentation crack driving force on the former. It has been shown that, as the segmentation crack spacing decreases, the magnitude of TSIF first decreases slightly; however when the segmentation crack spacing is smaller than a critical value, the decrease in TSIF with increasing crack density (i.e. decreasing crack spacing) is very significant, especially for large values of crack depth. Approximately, a single segmentation crack gives rise to the maximum TSIF for all possible crack depths. This phenomenon is the well-known shielding effect for parallel cracks [31,32]. The present investigation confirms the effectiveness of shielding for the case of thermal shock loading. Therefore, the reason why a segmented coating has higher durability than an intact one is that the former can cause the drop of crack driving force for segmentation crack propagation. It should be emphasized that until the segmentation crack density is high enough, can this beneficial effect be shown remarkably.

It is of much interest to estimate the admissible ambient temperature rise for the prevention of unstable crack propagation. It can be quantified by equating the calculated maximum TSIF to the fracture toughness of coating. For example, for the material pair in Table 1, under the most severe convection case (Bi→∞) and at the steady state, the functional relationship of Eq. (14) can be reduced to: $K_{max}/K_0=\Pi(s/h, l/h)$, with $K_0=E_1\alpha_1\theta_0\sqrt{h}/(1-\nu_1)$.

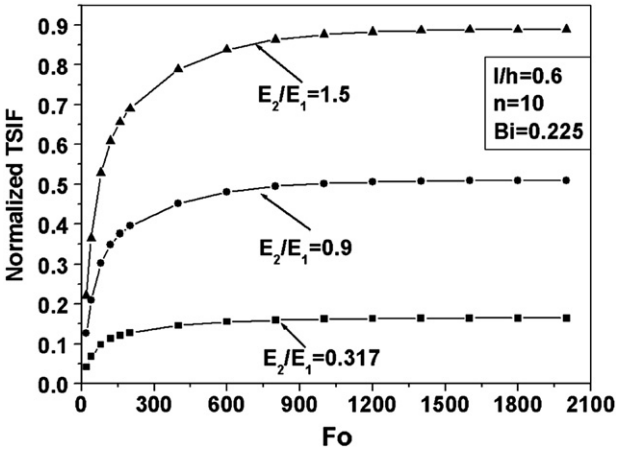

Fig. 11. The normalized TSIF versus normalized time for various modulus ratio. $l/h=0.6$, $n=10$, Bi=0.225. Other inputs are listed in Table 1.

By using $K_{max}=K_c$ (K_c is the fracture toughness of coating), the relationship between the admissible sudden temperature jump θ_0 and Π can be simply written as

$$\theta_0=\frac{\theta_c}{\prod} \tag{15}$$

with $\theta_c=\frac{K_c(1-\nu_1)}{E_1\alpha_1\sqrt{h}}$. The explicit expression is derived through the following fitting formula

$$\prod(s/h, l/h)=A_1-A_2\exp(-\beta\cdot s/h) \tag{16}$$

Some typical values of the unknown constants are determined as

$$A_1=0.14085, A_2=0.09732, \beta=0.69091, \text{for } l/h=0.4 \tag{17a}$$

$$A_1=0.15336, A_2=0.13130, \beta=0.66117, \text{for } l/h=0.5 \tag{17b}$$

$$A_1=0.16380, A_2=0.15164, \beta=0.60993, \text{for } l/h=0.6 \tag{17c}$$

Finally, the dependence of TSIF of segmentation crack on some material constants of interest has been considered. The effect of $\bar{\nu}=\nu_2/\nu_1$ has always little influence on the TSIFs and is therefore ignored [1]. The normalized TSIFs are plotted against dimensionless time in Fig. 11, for selected values of normalized Young's modulus E_2/E_1. It has been shown that the increase of modulus ratio can cause the increase of segmentation crack driving force and the possibility of unstable propagation. This effect was previously validated in the case of mechanical loadings [31]. The effect of normalized CTE, $\bar{\alpha}=\alpha_2/\alpha_1$, on the TSIFs can be deduced from Fig. 12. It indicates that for a given substrate, the increase of CTE of coating may lead to reduction for segmentation crack driving force. This dependency could be understood as follows: for a given substrate, the coating with higher CTE has

Table 2
Selected results for a homogeneous hollow cylinder, which is subjected to sudden heating from the inner surface while outer surface is kept at the initial temperature

$a/b=0.8$	F	0.00001	0.00005	0.0001	0.0003	0.0005	0.001
	$\bar{K}$	0.0042	0.0099	0.0139	0.0243	0.0314	0.0447
	$\bar{K}^1$	0.0038	0.0091	0.0129	0.0235	0.0306	0.0435
$a/b=0.66$	F	0.0005	0.002	0.008	0.02	0.04	
	$\bar{K}$	0.0142	0.0280	0.0581	0.0921	0.1213	
	$\bar{K}^1$	0.0137	0.0261	0.0567	0.0902	0.1201	

$n=2$, $W=b-a$, $l/W=0.03$, $F=Dt/a^2$, $\bar{K}=K/K_0$, $K_0=E\alpha\Delta T\sqrt{W}/(1-\nu)$. $\bar{K}$ and $\bar{K}^1$ are the result of current paper and Oliveira & Wu [6] respectively.

higher capability to accommodate thermal misfit strain, thus leading to the enhancement of coating durability.

6. Conclusions

In this paper, the thermally induced cracking of a segmented coating on the outer surface of a hollow cylinder has been considered, in which the segmentation cracks are modeled as a periodic array of axial edge cracks. Sensitivity analysis has been carried out to assess the effect of some important factors on the thermal stress intensity factors (TSIFs) for the propagation of multiple segmentation cracks. Results indicate that the TSIF is a monotonically increasing function of segmentation crack spacing. This result confirms that a segmented coating exhibits much higher thermal shock resistance than an intact counterpart, if only the segmentation crack spacing is narrow enough. The maximum TSIF is found to be at the steady state of thermal transient. As convection severity is increased, the maximum TSIF occurs earlier while its magnitude is kept unchanged. For a given substrate, the decrease of Young's modulus and/or increase of CTE of coating are conducive to the reduction of TSIFs, thus helpful for the durability enhancement of coating under thermal transients.

Acknowledgements

The authors gratefully acknowledge the financial support of the National Natural Science Foundation of China (Grant No. 10802007) and the Specialized Research Fund for the Doctoral Program of Higher Education of Ministry of Education (Grant No. 20070008003). We also want to express our deep gratitude to anonymous reviewers for their constructive suggestion.

References

[1] J.W. Hutchinson, Z. Suo, ASME Adv. Appl. Mech. 29 (1992) 63.
[2] H.H. Yu, M.Y. He, J.W. Hutchinson, Acta Mater. 49 (2001) 93.
[3] J.H. Underwood, A.P. Parker, G.N. Vigilante, P.J. Cote, ASME J. Press. Vessel. Technol. 125 (2003) 299.
[4] H.F. Nied, F. Erdogan, J. Therm. Stress. 6 (1983) 1.
[5] F. Delale, S.P. Kolluri, J. Therm. Stress. 8 (1985) 235.
[6] R. Oliveira, X.R. Wu, Eng. Fract. Mech. 27 (1987) 185.
[7] N. Noda, Y. Matsunaga, H. Nyuko, Int. J. Press. Vessel. Piping 42 (1990) 247.
[8] M. Perl, A. Ashkenazi, Eng. Fract. Mech. 41 (1992) 597.
[9] M. Perl, A. Ashkenazi, Eng. Fract. Mech. 42 (1992) 747.
[10] K.Y. Lee, J.S. Kim, Eng. Fract. Mech. 56 (1997) 423.
[11] H.F. Nied, Eng. Fract. Mech. 20 (1984) 113.
[12] R. Tang, F. Erdogan, ASME J. Eng. Gas Turbine Power 107 (1985) 212.
[13] C.K. Chen, B.L. Kuo, Eng. Fract. Mech. 49 (1994) 381.
[14] X. Chen, K. Zhang, G. Chen, G. Luo, Int. J. Solids Struct. 43 (2006) 6424.
[15] J.H. Kim, M.C. Kim, C.G. Park, Surf. Coat. Technol. 168 (2003) 275.
[16] J.L. He, K.C. Chen, Surf. Coat. Technol. 200 (2005) 1464.
[17] Y.Z. Tsai, J.G. Duh, Surf. Coat. Technol. 200 (2005) 1683.
[18] Y. Hu, K. Zhang, G.N. Chen, C.W. Wu, J. Metal Treatment 30 (2005) 161 (Suppl.) (in Chinese).
[19] K. Zhang, C.W. Wu, Y. Hu, G.N. Chen, Solid State Phenom. 118 (2006) 243.
[20] G.N. Chen, G.X. Luo, K. Zhang, et al., Acta Armament. 24 (2003) 6 (Suppl.) (in Chinese).
[21] X. Chen, G. Chen, K. Zhang, G. Luo, J. Xiao, Surf. Coat. Technol. 202 (2008) 2878.
[22] B. Zhou, K. Kokini, Surf. Coat. Technol. 187 (2004) 17.
[23] B. Zhou, K. Kokiki, Acta Mater. 52 (2004) 4189.
[24] E. Sternberg, J.G. Chakravorty, ASME J. Appl. Mech. 26 (1959) 503.
[25] T. Atarashi, S. Minagawa, Int. J. Eng. Sci. 30 (1992) 1543.
[26] H.S. Carslaw, J.C. Jaeger, Conduction of Heat in Solids, Oxford University Press, Oxford, 1986.
[27] Ansys: Guidance to structural analysis (V.0205), Ansys Inc., 2000.
[28] P.P. Lynn, A.R. Ingraffea, Int. J. Numer. Methods Eng. 12 (1978) 1031.
[29] G.I. Barenblatt, Scaling, Self-similarity, and Intermediate Asymptotics, Cambridge University Press, Cambridge, 1996.
[30] Q.F. Ma, R.S. Fang, L.C. Xiang, S. Guo, Practical Handbook of Thermophysical Properties, Chinese Agricultural Press, Beijing, 1986 (in Chinese).
[31] G.W. Schulze, F. Erdogan, Int. J. Solids Struct. 35 (1998) 3615.
[32] A.P. Parker, Eng. Fract. Mech. 62 (1999) 577.